Extension of the Hot-Switching Reliability of RF-MEMS Switches Using A Series Contact Protection Technique

Yuhao Liu, *Student Member, IEEE,* Yusha Bey, and Xiaoguang Liu, *Member, IEEE*

***Abstract*—This paper presents a design methodology for drastically improving the hot-switching reliability of contact-type radio frequency micro-electromechanical (RF-MEMS) switches. In the proposed design, sacrificial contacts are placed in parallel with low-resistance contacts to significantly reduce the electric field across the latter. The lower field strength drastically reduces the contact degradation associated with field induced material transfer. Theoretical and numerical modeling show that the proposed protection scheme introduces minimal, if any, impact on the switch's RF performance. To realize the protection scheme, we introduce a novel mechanical design that allows the correct protection actuation sequence to be realized using a single actuator and bias electrode. As a demonstration, several 0–40 GHz RF-MEMS switches are fabricated using a robust copper sacrificial layer technique. Compared with unprotected switches, the protected switch design exhibits over 100 times improvement in hot-switching lifetime. In particular, we demonstrate 100–150 million cycle lifetime at 1 W hot-switching and 50 million cycles at 2 W hot-switching before catastrophic failure, measured in open-air lab environment. Further optimization of the structural design and contact materials is likely to further increase the hot-switching lifetime.**

***Index Terms*—MEMS switch, RF micro-electromechanical systems, contact protection, MEMS reliability, hot-switching**

I. Introduction

DUE to its low insertion loss, high isolation, high linearity, wide bandwidth, and near-zero dc power consumption, radio frequency micro-electromechanical (RF-MEMS) switch has been an emerging technology that can be used in automated test equipment (ATE), wide-band instrumentation, switching matrice, digital attenuators, satellite switching networks and defense systems to achieve superior system performance. RF-MEMS switches have superior RF performance over traditional electromechanical relays, p-i-n diodes, and field effect transistor (FET) switches [1]. In addition, RF-MEMS switches can be fabricated on virtually any substrate, allowing them to be integrated with existing semiconductor processes.

Compared with capacitive RF-MEMS switches, metal contact type switches have large bandwidth from dc to RF frequency and are favored in many wide-band applications [2], [3]. Over the years, several companies and research groups have demonstrated RF-MEMS metal contact switches with excellent performance [4]–[8].

However, the reliability issues associated with RF-MEMS contact switches have been a barrier for wider adoption of the technology [9]. The main failure mechanism for contact switches is contact degradation [10], which can be attributed to a variety of physical and chemical processes, including welding [11], stiction [12], bridge transfer [13], field-induced material transfer [14] and carbon deposition [15]. In the past, significant efforts have been devoted to boost the lifetime (primarily in terms of cycling time) of RF-MEMS contact switches. For example, the Radant MEMS switch can be cycled up to 1.5 trillion times [16] and the Sandia MEMS switch was cycled up to 10 billion times [17]. However, both switches were characterized under the cold-switching condition, in which the RF power is turned off before switching events occur. Under hot-switching conditions, in which switches are turned on and off while the RF power is kept on, the reliability of these switches degrades quickly with a sharp increase in contact resistance and insertion loss after a few tens of thousands of cycles. For applications where hot-switching is needed [18], improving the hot-switching reliability of RF-MEMS switches has been a significant challenge.

Several previous works have reported field induced material transfer damage mechanisms in hot-switching condition [19]–[21]. The common damage mechanisms include field evaporation, field emission, arc or pseudo-arc material transfer, and ohmic heating/bridge material transfer. These mechanisms are the result of a local potential difference caused by the RF voltage which is not observed in cold-switching conditions. Thus, hot-switching lifetime is usually significantly short than that under the cold-switching condition.

Several methods for improving the hot-switching reliability of RF-MEMS switches have been reported. One way is to use dissimilar contact materials (Au/Ru) rather than (Au/Au). Dissimilar contact materials will have less material transfer between each other than between the same material. The switch can be cycled up to 100 million cycles under 100 mW [22]. Another design uses a ball grid array (BGA) dimple design [23]. The contact dimple has a ball shape, and high electric fields that could cause arcing only happen near the tip of the contact dimple. Because of the high packing density, the BGA design could suppress the arcing-induced contact failure with field screening as well as the local mechanical deformation of each dimple. The fabricated switch can be cycled up to 100 million

Y. Liu and X. Liu are with the Department of Electrical and Computer Engineering, University of California at Davis, Davis, CA 95616 USA (e-mail: yuhliu@ucdavisedu.edu; lxgliu@ucdavis.edu).

Y. Bey is with the Center for Nano-MicroManufacturing, University of California at Davis, Davis, CA 95616 USA (e-mail: jasmall@ucdavis.edu).

The authors would like to thank National Science Foundation for supporting this research.

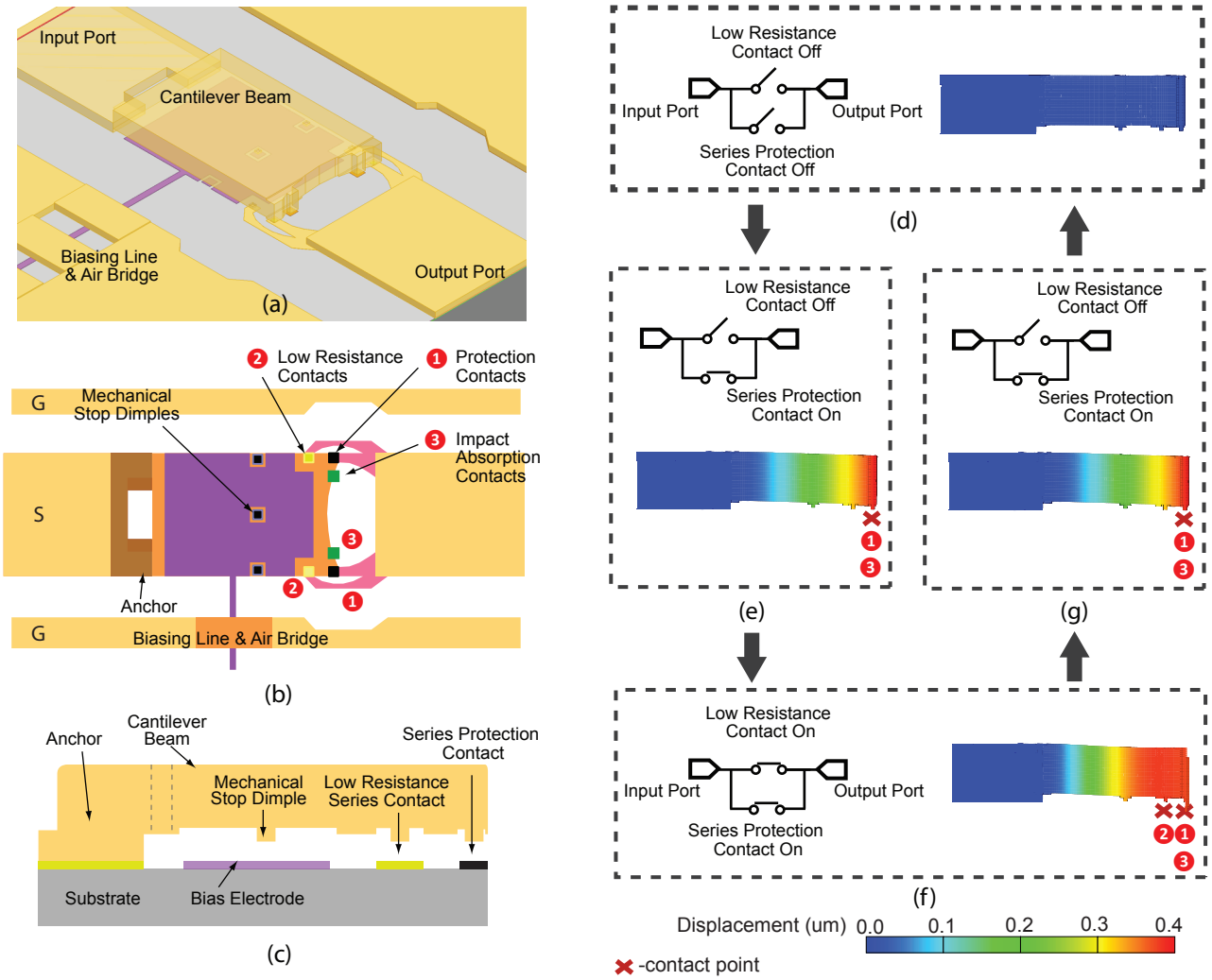

Fig. 1. Concept of RF-MEMS switch with series protection contact : (a) 3-D view; (b) Top view; (c) Profile view; (d) Off-state; (e) Transition-state from off-state to on-state; (f) On-state; (g) Transition-state from on-state to off-state.

cycles under 1 W, but there is no report on how the contact resistance changes over the cycling test.

In this paper, we demonstrate a methodology for drastic improvement of RF-MEMS switches' hot-switching reliability. In particular, we show that by employing a protective contact in parallel with a series RF-MEMS switch, the hot-switching lifetime can be extended by more than two orders of magnitude while maintaining excellent RF performance. In the past, we have proposed a similar concept which uses a protective contact in shunt and also improves the off-state isolation performance [24]. However, hot-switching lifetime characterization results were not presented. In [25] and [26], Song et al. demonstrated similar techniques that improved the hot-switching lifetime to 2 million cycles under 100 mW dc power. However, the demonstrated switches were not designed for high frequency operation and no RF characterization was presented.

In this paper, we present theoretical analysis of the performance and design trade-offs of the proposed hot-switching reliability improvement methodology for RF-MEMS switches. We introduce a novel mechanical design that allows the correct protection actuation sequence to be realized using a single actuator. A robust copper sacrificial layer process was also introduced to ensure the reliability and yield of the switch fabrication.

II. Device Concept

Fig. 1 shows the proposed switch design and its working principles. Fig. 1 (b) shows the top view of the switch. The movable part of the switch is a rectangular-shaped cantilever beam placed in series between the input and output signal lines. There are three groups of contact dimples towards the tip of the cantilever. The first group of contacts (labeled number 1) are placed at the very tips of the cantilever and serves as protection contacts that will be degraded during hot-switching events. The second group of contacts (labeled number 2), which are placed a distance away from the tip of the cantilever, provide low series on-state resistance. Both group 1 and 2 connect the input and output signal lines. The third group of contacts (labeled number 3) provide additional mechanical impact absorption and are not connected to the signal lines. In

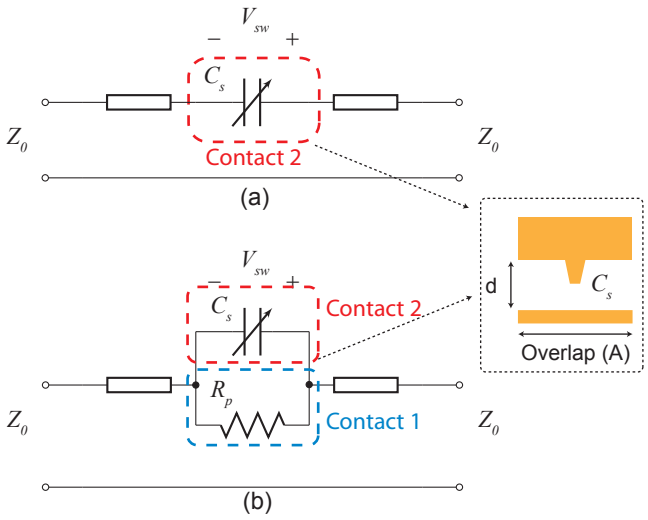

Fig. 2. Equivalent circuit model of switches with protection and without protection.

addition, three mechanical stopper contacts are placed in the middle of the biasing electrode only to prevent catastrophic contact between the cantilever and the electrode as there is no dielectric on top of the biasing electrode to prevent charging issues. These stopper contacts are not normally touched during switching cycles. The contact force will be concentrated on the conducting contacts to achieve lower contact resistance.

A. OFF-state to ON-state

In one switching cycle, the switch is initially in the off-state [Fig. 1 (d)]. As the bias voltage increases, the switch will close the protection contacts ① and impact absorption contacts ③ first [Fig. 1 (e)].At this stage, most of RF power will pass through the protection contacts ① and the voltage difference between the low-resistance contacts ② and the output signal line is significantly lower than that in the case of no protection.

To see the protection mechanism quantitatively, we resort to the equivalent circuit modeling of the switch. Fig. 2 (a) shows the equivalent circuit of a series contact switch *without protection*. Before contact is made, the switch can be modeled as a series connected capacitor whose capacitance C_s is dependent on the overlap area A and separation d between the tip of the cantilever and the opposing RF electrode. To simplify the model, the series inductance and parasitic (mostly fringing-field) capacitance are omitted. We also assume that the contact dimple area is far less than A and contribute little to C_s.

The S-parameters for Fig. 2 (a) is

$$S_{11} = S_{22} = \frac{1}{1 + 2j\omega Z_0 C_s}, \tag{1}$$

$$S_{12} = S_{21} = \frac{2j\omega Z_0 C_s}{1 + 2j\omega Z_0 C_s}, \tag{2}$$

where ω is the angular frequency of the RF signal, and Z_0 is the characteristic impedance of the transmission line.

The voltage across the switch contacts with an input power of P is

$$V_{sw} = V_1^- + V_1^+ - V_2^- = (S_{11} + 1 - S_{12})V_1^+, \tag{3}$$

where $V_1^+ = \sqrt{2PZ_0}$ is the amplitude of the incident wave (from the input port), V_1^- the amplitude of the reflected wave, V_2^- the amplitude of the transmitted wave, and P is the input power.

Therefore, the voltage $V_{sw,u}$ across the unprotected switch is

$$V_{sw,u} = \sqrt{\frac{8PZ_0}{4Z_0^2\omega^2 C_v^2 + 1}}. \tag{4}$$

The electric field intensity will be:

$$E_{sw} = \frac{V_{sw,u}}{d} = \sqrt{\frac{8PZ_0}{4Z_0^2\omega^2\epsilon_0^2 A^2 + d^2}}. \tag{5}$$

Fig. 2 (b) shows the equivalent circuit of the *protected* switch with the protection contacts which are modeled as a resistor R_p in parallel with the switch capacitance C_s. The contact resistance is assumed to be constant even though the resistance will drop as the biasing voltage increases. Following the same procedure as in (1)–(5), we can calculate the voltage across the *protected* switch contact.

$$V_{sw,p} = \sqrt{\frac{8PZ_0}{4Z_0^2\omega^2 C_s^2 + \left(\frac{2Z_0}{R_p} + 1\right)^2}}. \tag{6}$$

The electric field intensity will be:

$$E_{sw} = \frac{V_{sw}}{d} = \sqrt{\frac{8PZ_0}{4Z_0^2\omega^2\epsilon_0^2 A^2 + d^2\left(\frac{2Z_0}{R_p} + 1\right)^2}}. \tag{7}$$

To evaluate the difference between (5) and (7), actual device dimensions (Section III-A) are used to illustrate the model. The area A is $56.25\,\mu\text{m}^2$ and d varies from $0.9\,\mu\text{m}$ to $0.5\,\mu\text{m}$ when contact is made between the dimples.

Fig 3 illustrates the modeled electric field intensity between contacts ② with respect to d under 1 W input power and various R_p values. The unprotected switch has the highest electric field intensity of $39.9\,\text{V}/\mu\text{m}$. The switch with $2\,\Omega$ R_p has the lowest electric field intensity of $0.78\,\text{V}/\mu\text{m}$, representing a more than 50 times reduction in electric field intensity and making the switch much less prone to hot-switching damages. The electric field intensity tends to go up as the R_p increases so it is preferable to achieve a low R_p. In essence, a local cold switching condition is created by shorting the low-resistance contacts out with the protection contacts.

During the lifetime of the switch, the protection contacts ① will be degraded by hot-switching and R_p will increase and gradually provide less protection for the contacts ①. However, even if R_p increases to $50\,\Omega$ the electric field intensity would still be only one fourth of that of the unprotected switch (Fig.3 (a)). Therefore, in practice, failure mechanisms like stiction may occur long before the protection contacts lose their efficiency.

Fig. 4 compares the electric field across the low-resistance contacts ② with [Fig. 4-(b)] and without [Fig. 4-(a)] the protection contacts. The calculations show that even for a relatively large protection contact resistance of 50 Ω, the electric field across the low-resistance at 10 W RF power is at the same level as that of an unprotected contacts at 1 W.

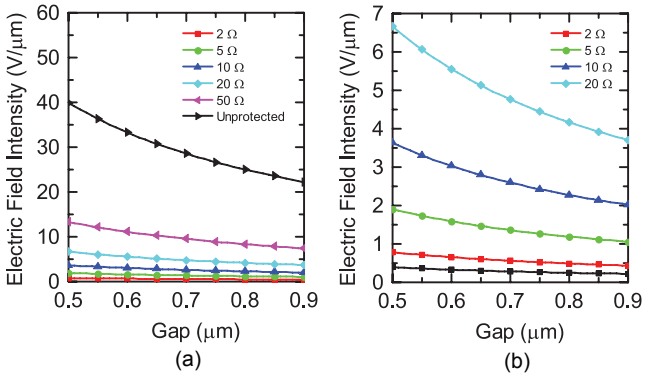

Fig. 3. (a) Calculated electric field intensity of unprotected switch and switches with different protection contact resistances (at RF Frequency of 2.4 GHz). (b) Zoom-in view of (a) for low protection contact resistance.

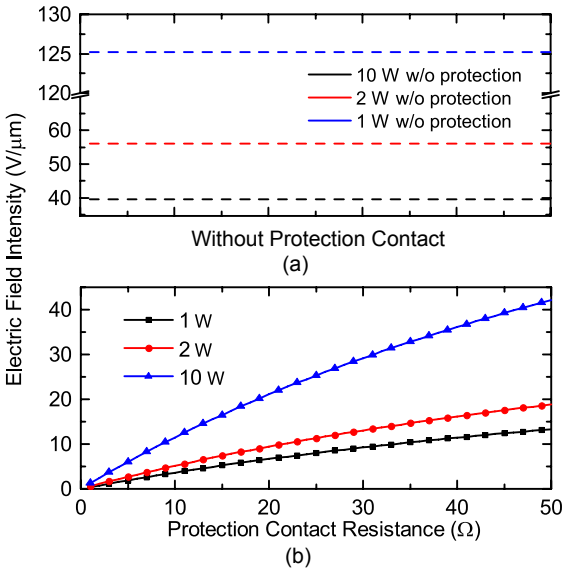

Fig. 4. (a) Calculated electric field intensity under different input power levels at 2.4 GHz at the closest gap (0.5 μm) without the protection contacts; (b) Calculated electric field intensity under various input power levels at 2.4 GHz at the closest gap (0.5 μm) with respect to different protection contact resistances.

As the biasing voltage increases, the low-resistance contacts are closed. The switch transitions to the on-state. RF power will be distributed between contacts ① and ②. However, contacts ② are designed to have low resistance so that most of the RF power will pass through them, achieving low insertion loss.

B. ON-state to OFF-state

When toggling from the on-state to off-state, the low resistance contacts will still be protected from high, and potentially damaging, electric fields. When reducing the electrostatic bias, the beam will release in a way that will allow the low resistance contacts to detach before the high resistance/protective contacts. This results in safely transferring the RF power to the protection contacts, thereby allowing the low resistance contacts to open in a nearly cold-switch condition. In the on-state the cantilever is largely bent, so the restoring force is relatively high to prevent contact adhesion. As the biasing voltage further decreases, the protection contacts will detach and the switch will transition to the off-state. The electric field change will be the same as that from off-state to on-state. During this sequence, the low-resistance contacts are still protected from the high electric field.

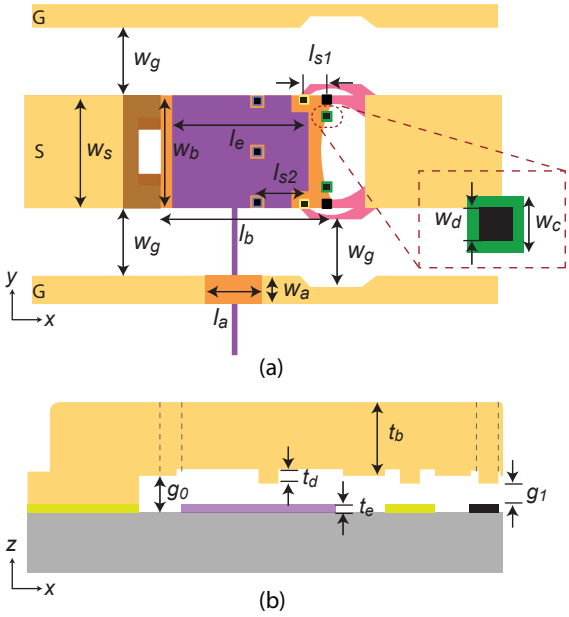

Fig. 5. Dimensions of the proposed switch. (a) Top view; (b) Side view.

III. Switch Design and Modeling

A. Switch Geometries

Fig. 5 reprints Fig. 1 (b)&(c) with the critical dimensions of the switch labeled. The cantilever beam is 150 μm × 100 μm, while the overall switch occupies 150 μm × 200 μm. The switch is designed on a 50 Ω coplanar waveguide (CPW) line. The protection contacts are connected directly from underneath the beam to the output port. The low-resistance contacts are connected from the outside of the beam. The ground planes of the CPW line are cut to match the impedance of the connecting line of the low-resistance contacts. The separation between the low-resistance contacts and the series protection contacts is chosen such that the actuation voltages of the two types of contacts are largely different. In this case the protection contacts will have enough time to settle and protect the low-resistance contacts. There is a trade-off, however, between the difference of the actuation voltages and the restoring force of the protection contacts. We will discuss the trade-off in the mechanical analysis section. There

TABLE I
GEOMETRY PARAMETERS OF THE SWITCH

Geometry parameter	Symbol	Value (μm)
CPW line width	w_s	100
CPW line gap	w_g	60
Beam width	w_b	100
Dimple width	w_d	2.5
Contact width	w_c	7.5
Air bridge width	w_a	20
Beam length	l_b	150
Electrode length	l_e	120
Air bridge length	l_a	60
Protection and low-resistance contact separation	l_{s1}	20
Stopper and low-resistance contact separation	l_{s2}	40
Beam thickness	t_b	5
Dimple thickness	t_d	0.5
Biasing electrode thickness	t_e	0.15
Cantilever to electrode gap	g_0	0.9
Dimple to contact gap	g_1	0.4

is no biasing electrode from series protection contacts to low-resistance contacts. This configuration will distribute more contact force on low-resistance contacts to achieve lower contact resistance at on-state. Finally, to facilitate dc biasing of the switch and to reduce undesired RF leakage, air bridges are formed to allow the biasing line to pass through the ground plane.

B. Mechanical Design and Simulation

The cantilever beam of the switch can be analyzed using the Euler-Bernoulli beam equation [27]:

$$\frac{M}{EI} = -\frac{d^2v}{dx^2}, \tag{8}$$

$$I = \frac{w_b t_b^3}{12}, \tag{9}$$

where $E = 79\,\text{GPa}$ is Young's Modulus of gold, I is the moment of inertia of the beam, and v is the deflection of the beam in z direction. The biasing electrode puts an even load on part of the beam. The load distribution (N/m) q can be expressed as [28]:

$$q = \frac{\epsilon_0 w_b V_a^2}{g_0^2}, \tag{10}$$

where ϵ_0 is the vacuum permittivity, V_a is the applied bias voltage, and g_0 is the gap between the beam and the electrode.

In the following analysis, it is assumed that the load distribution q is constant across the cantilever neglecting the bending of the cantilever to get a simplified analytical solution of the beam profile. This assumption is valid when the biasing electrode is relatively far away from the cantilever and the change in the gap between the cantilever and the biasing electrode is small.

Before the protection contacts close, the boundary conditions are

$$v(x)|_{x=0} = 0,$$

$$\left.\frac{dv(x)}{dx}\right|_{x=0} = 0,$$

$$v(x)|_{x=l_e-} = v(x)|_{x=l_e+},$$

$$\left.\frac{dv(x)}{dx}\right|_{x=l_e-} = \left.\frac{dv(x)}{dx}\right|_{x=l_e+}.$$

The displacement of the beam can then be calculated as:

$$v(x) = \begin{cases} \dfrac{qx^2}{24EI}\left(6l_e^2 - 4l_e x + x^2\right), & 0 < x \leqslant l_e \\ \dfrac{ql_e^3}{24EI}\left(4x - l_e\right). & l_e \leqslant x \leqslant l_b \end{cases} \tag{11}$$

When the protection contacts close, an additional boundary condition applies:

$$v(x)|_{x=l_b} = g_1. \tag{12}$$

In this case, the displacement can be solved as:

$$v(x) = \begin{cases} \dfrac{qx^2}{24EI}\left(6l_e^2 - 4l_e x + x^2 - \dfrac{12F_1 l_b}{q} + \dfrac{4F_1 x}{q}\right), & 0 < x \leqslant l_e \\ \dfrac{1}{24EI}\left(4F_1 x^3 - 12F_1 l_b x^2 + 4ql_e^3 x - ql_e^4\right). & l_e \leqslant x \leqslant l_b \end{cases} \tag{13}$$

We can also express the contact force F_1 on the protection contacts as:

$$F_1 = \frac{4ql_e^3 l_b - ql_e^4 - 24EIg_1}{8l_b^3}. \tag{14}$$

When the low-resistance contact is closed, the following boundary condition is applied:

$$v(x)|_{x=l_e} = g_1. \tag{15}$$

The contact forces on both protection contacts F_1 and low-resistance contacts F_2 can be written as:

$$F_1 = \frac{A_2A_5 - A_4A_3}{A_2^2 - A_1A_3}, \tag{16}$$

$$F_2 = \frac{A_2A_4 - A_1A_5}{A_2^2 - A_1A_3}, \tag{17}$$

where

$$\begin{aligned} A_1 &= -8l_b^3, \\ A_2 &= 4l_e^3 - 12l_b l_e^2, \\ A_3 &= -8l_e^3, \\ A_4 &= 24EIg_1 - 4ql_e^3 l_b + ql_e^4, \\ A_5 &= 24EIg_1 - 3ql_e^4. \end{aligned}$$

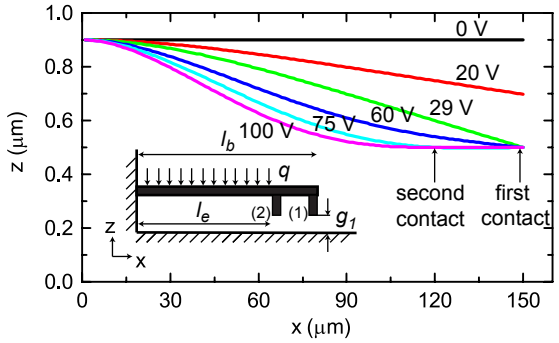

Fig. 6. Beam profile predicted by theoretical model under different biasing voltages.

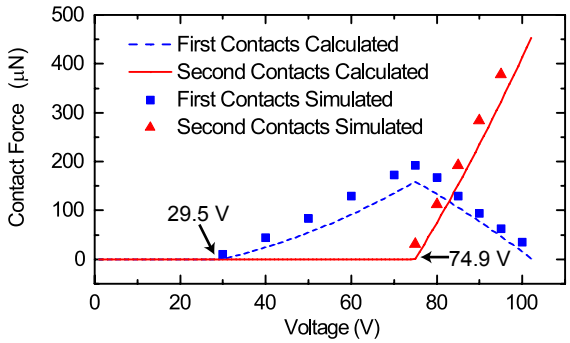

Fig. 7. Calculated and simulated contact force under different biasing voltages.

The displacement in this region can be calculated as:

$$v(x) = \begin{cases} \frac{1}{24EI}\left(6ql_e^2x^2 - 4ql_ex^3 + qx^4 \right. \\ \quad -12F_2l_ex^2 + 4F_2x^3 \\ \quad \left. -12F_1l_bx^2 + 4F_1x^3\right), & 0 < x \leqslant l_e; \\ \frac{1}{24EI}\left(4F_1x^3 - 12F_1l_bx^2 + 4ql_e^3x \right. \\ \quad \left. -12F_2l_e^2x + 4F_2l_e^3 - ql_e^4\right), & l_e \leqslant x \leqslant l_b. \end{cases} \tag{18}$$

The calculated beam profile is plotted in Fig 6. The geometry parameters used in the calculations are the same as used in switch design. By increasing the voltage, the beam is bent making contacts sequentially. The actuation voltage for the first contact is 29.5 V and for the second contact is 74.9 V.

The contact sequence can also be understood from the contact forces (Fig. 7). Because there is no biasing electrode between contacts ① and ②, the contact force is concentrated on the contacts ② to achieve lower contact resistance. It can be seen Fig. 7 that the protection contacts experience the largest contact force just before the low-resistance contacts close when the actuation voltage increases, the contact force on the protection contacts gradually decreases and is transferred to the low-resistance contacts. If the bias voltage further increases, the protection contacts will detach leaving the low-resistance contacts as the only contacts for the switch. This will give a way to open the protection contact to recover the switch from stiction on the protection contacts.

When qualitatively designing the switch actuator, the protection contact dimple always will be positioned closest to the free end of the cantilever (please refer to Fig. 1(b) and (c)). The low resistance contact will always be offset further back from the cantilever free end, in the direction of the anchor. In this configuration, the protection contacts will always close first. The restoring force on the protection contact is dependent on distance between the protection contact to low-resistance contact by:

$$F_r = \frac{24EIg_1}{3l_e^3 + 4l_e^3x_d} \tag{19}$$

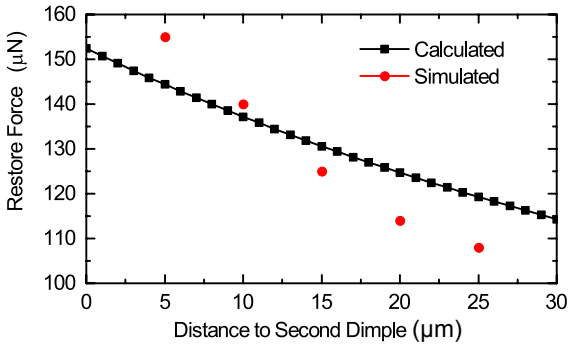

Fig. 8. Calculated and simulated restoring force of protection contact for different dimple positions.

where x_d is the distance from the protection contacts to the low-resistance contacts. Fig. 8 shows restoring forces for different protection contact positions. The restoring force is the highest when the protection contact are placed next to the low-resistance contacts and the force decreases as the distance increases. High restoring force can counteract stiction, but the time interval between forming protection contacts and forming low-resistance contacts will be shorter if the two contacts are placed closer to each other. If the protection contacts are not mechanically damped, some settling time is needed before they reach a steady state. If the actuation interval between the protection contacts and the low-resistance contacts is not long enough, the low-resistance contacts may still see high RF power before the protection contacts settle and hot-switching damage is likely to happen on the low-resistance contacts. In this design we place the protection contacts $30\,\mu\mathrm{m}$ away from the low-resistance contacts.

The induced stress in the MEMS structure also needs to be studied and controlled to ensure reliable operation. Due to viscoelasticity and creep effects the material properties will drift during actuation [29]. This effect will lead to unexpected biasing voltage changes and reduce the reliability of the switch. Since the switch will be operating with a large degree of bending, the induced stress has to be kept minimum. The induced stress at the beam anchor has been minimized with an opening which also serves as a release

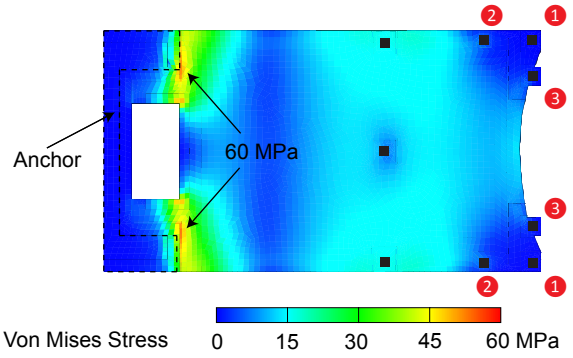

Fig. 9. Simulated Von Mises Stress under 90 V actuation voltage.

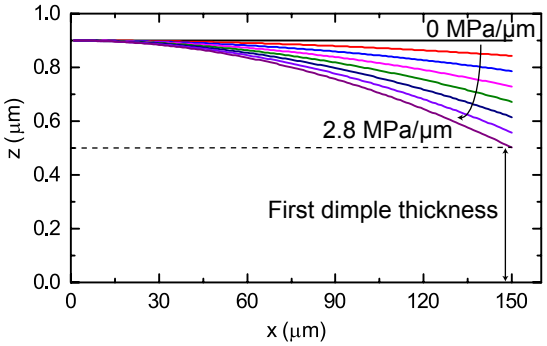

Fig. 10. Beam deflection due to positive stress gradient.

hole for sacrificial layer removal. Fig.9 shows the simulated Von Mise stress for the switch under 90 V actuation voltage using the Coventorware [30] FEM solver. The maximum stress is 60 MPa at the switch anchor.

Cantilever based MEMS switches are highly susceptible to stress gradients. Stress gradients can result in undesired beam deflections, which typically leads changes in the actuation voltage (beam bending up) and sometimes a completely unusable device (beam bending in down position and touching the bottom electrode right after releasing). The axial stress in the beam before release is:

$$\sigma = \sigma_0 - \frac{\sigma_1}{t_b/2} z, \tag{20}$$

where σ_0 is the average compressive stress in the beam and σ_1 is the stress difference through the thickness of the beam. A linear stress gradient is assumed here. The internal momentum due to stress gradient can be calculated as:

$$M_x = \int_{-t_b/2}^{t_b/2} w_b z \sigma dz = -\frac{1}{6} w_b t_b^2 \sigma_1. \tag{21}$$

By solving the Euler-Bernoulli beam equation, the beam deflection due to the stress gradient is:

$$v(x) = \frac{1}{12} \frac{w_b t_b^2 \sigma_1 x^2}{EI}. \tag{22}$$

Then, the total beam deflection is:

$$v(x) = \begin{cases} \dfrac{qx^2}{24EI}\left(6l_e^2 - 4l_e x + x^2\right) + \dfrac{1}{12}\dfrac{w_b t_b^2 \sigma_1 x^2}{EI}, \\ \qquad\qquad 0 < x \leqslant l_e; \\ \dfrac{ql_e^3}{24EI}\left(4x - l_e\right) + \dfrac{1}{12}\dfrac{w_b t_b^2 \sigma_1 x^2}{EI}, \\ \qquad\qquad l_e \leqslant x \leqslant l_b. \end{cases} \tag{23}$$

Fig. 10 shows the deflection due to positive stress gradient when there is no biasing voltage. The first contact dimple will touch the bottom electrode when the stress gradient is larger than 2.8 MPa/μm. The switch will be constant ON, leading to a permanent device failure. Fig. 11 plots the first and second contact dimple displacement under different actuation voltage with different negative stress gradient. With negative stress gradient, the beam will bend up and the first contact

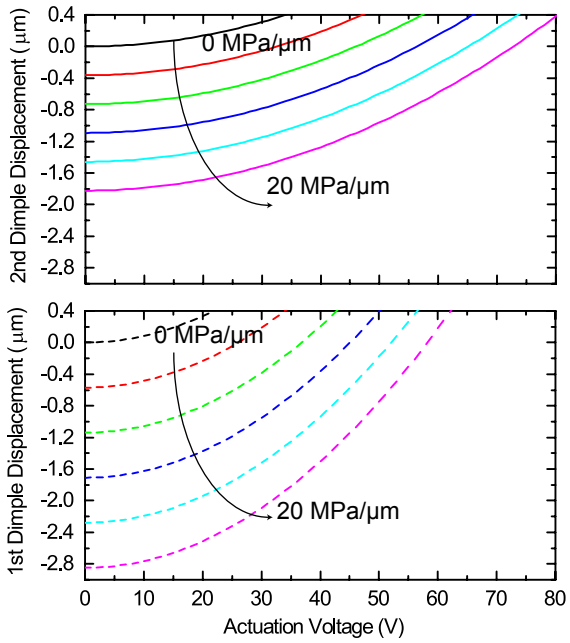

Fig. 11. First and second contact dimple movement under different actuation voltage with different negative stress gradient.

dimple will always have larger displacement upward than the second contact dimple. However, when the actuation is applied the first contact dimple will always travel 0.4 μm to make contact with the bottom electrode first. The sequence that the protection contact will close first can be achieve even with a negative stress gradient up to 20 MPa/μm. In our fabrication process the stress gradient was kept low and the beam is an intrinsic layer of plated gold. Neither permanent ON nor change of actuation sequence was observed in the experiment.

C. EM Analysis

The RF performance of the switch geometry is analyzed and optimized in Ansys HFSS [31] (Fig. 12). The isolation is 23 dB at 6 GHz in the off-stage. Because the protection contacts introduce additional overlap area between the cantilever and the bottom RF electrodes, the isolation performance is compromised for hot-switching protection. The insertion loss of the switch is 1.31 dB at 6 GHz when only the protection

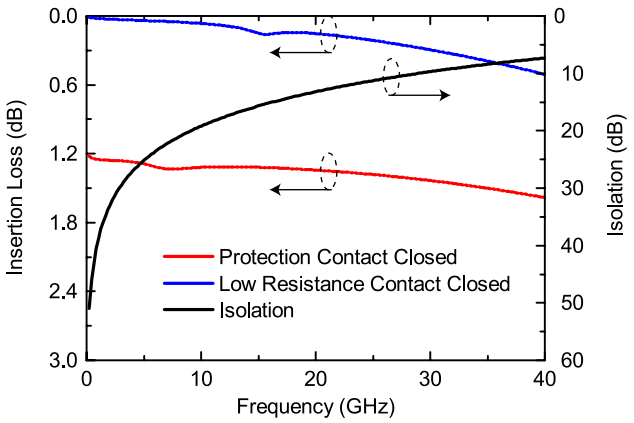

Fig. 12. Simulated insertion loss and isolation for different switching stages.

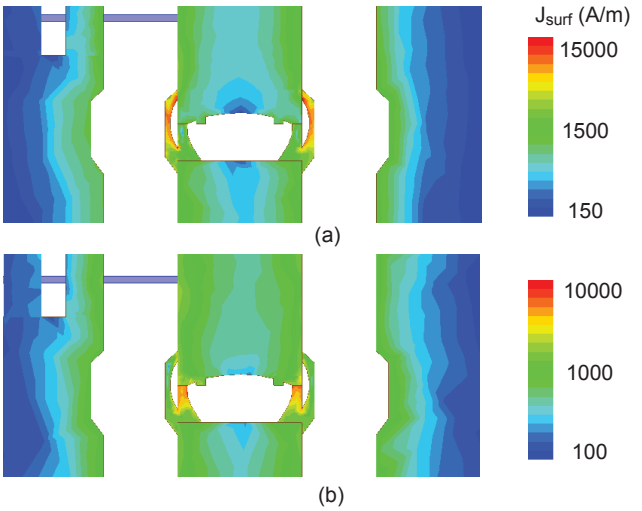

Fig. 13. Simulated surface current distribution (a) when the protection contacts are closed, and (b) when the low-resistance contacts are closed.

contacts are closed and is lowered to 0.04 dB when the low-resistance contacts are closed. To demonstrate the RF power redistribution, Fig. 13 compares the simulated current distributions of the two stages. It is clear that the current is concentrated on the protection contacts in the protection stage and transfers to the low-resistance contacts when they close.

IV. Device Fabrication

Fig. 14 shows the fabrication process for the switch, modified from [24]. The switch is fabricated on a high resistivity (∼10 kΩ-cm) oxidized silicon substrate. A 150 nm thick high resistance (∼ 1 kΩ/□) silicon chrome (SiCr) dc bias line is first patterned by lift-off [Fig. 14 (a)]. Next, a second lift-off is used to pattern the 150 nm thick bottom gold (Au) contacts with a titanium (Ti) adhesion layer [Fig. 14 (b)]. The protection contacts are patterned using a lift-off process. The 100 nm thick protection contacts are made of platinum (Pt) with Ti as the adhesion layer [Fig. 14 (c)]. A 400 nm thick copper (Cu) sacrificial layer with chromium (Cr) as the adhesion metal is sputtered and patterned with a liftoff process [Fig. 14(d)]. A second 500 nm thick Cr/Cu sacrificial layer is deposited and

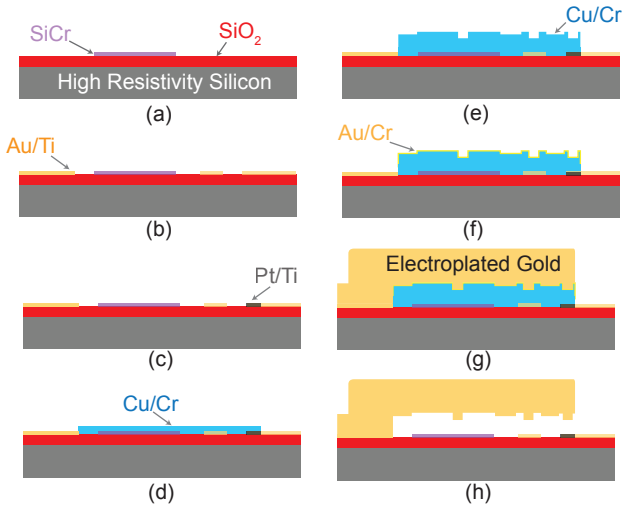

Fig. 14. Fabrication process of the switch.

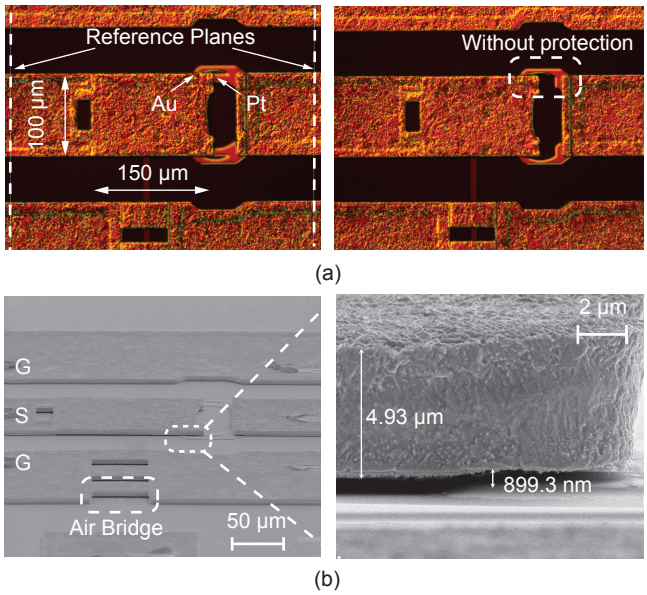

Fig. 15. (a) Optical images of a pair of protected and unprotected switch, (b) Scanning electron microscope (SEM) image of the fabricated switch.

patterned to form the cantilever dimple mold [Fig. 14 (e)]. A 50/150 nm Cr/Au is sputtered as the seed layer for the subsequent electroplating. Positive photoresist is spin-coated to 6 µm and patterned to form the electroplating mold for the cantilever. The cantilever is then electroplated to 5 µm thick [Fig. 14 (g)]. The contact dimples are also electroplated and formed in gold in this step. The electroplating mold and gold seed layer are removed in their respective dedicated etchants before the devices are released in the chromium etchant and dried in the critical point dryer [Fig. 14 (f)]. The chromium etchant is used to etch away all the copper sacrificial layers and chromium adhesion layers at the same time. The Cu sacrificial process avoids using any polymer as the sacrificial layer to minimize potential carbon contamination [15].

Fig. 15 shows optical and scanning electron microscopy (SEM) images of the fabricated switch. Fig. 15(a) shows

images of a protected switch and an unprotected switch used as a control device. The unprotected switch is essentially the same as the protected switch except that the protection contacts are not connected to the signal line.

V. Measurement and Discussion

A. Actuation voltage

The protected switch has two actuation stages. The actuation voltage of one protected switch is measured. The actuation voltage for the protection contacts is 29 V and for the low-resistance contacts is 82 V. This result is in good agreement with the modeling (29.5 V and 74.9 V respectively).

B. S-parameters

The small-signal RF performance of the fabricated switches was measured using an HP 8722D network analyzer with Ground-Signal-Ground (GSG) microwave probes. On-wafer Through-Reflection-Line (TRL) standards were used for calibration to the reference planes indicated in Fig. 15 (a). One switch with protection contacts and another without protection contacts were measured for comparison.

The S-parameter measurement results are shown in Fig. 16. The transition-state data is taken when the protection contacts are closed on the protected switch. The insertion loss is 1.46–2.65 dB in the 0–40 GHz range. The on-state data is taken when the low-resistance contacts are actuated at 90 V. The insertion loss decreases to 0.11–0.62 dB in the 0–40 GHz range. The insertion loss for the unprotected switch, actuated at 90 V, is 0.32–0.74 dB in the 0–40 GHz range. The protected switch has lower insertion loss in general due to additional conducting contacts. The isolation for the protected switch is 36.8–8.1 dB, and for the unprotected is 38–9.6 dB, both measured in the 0–40 GHz range. The protected switch has poorer isolation due to more overlap between actuator and contact electrode because of the additional protection contacts. The measured and simulated isolation has a 3 dB discrepancy due to an unintended expansion of contacts and dimple sizes in the device fabrication.

C. Linearity

The linearity of the MEMS switch was measured at a center frequency of 2.4 GHz. Fig. 17 shows the test setup for a two-tone measurement. The two tones were 25 MHz offset from the center frequency. The input power level varied from 12 dBm to 16 dBm. The spectrum analyzer is set to 20 dB input attenuation to ensure that the nonlinearity of the equipment does not introduce appreciable measurement errors. The third-order inter-modulation intercept point (IIP3) of the device is 64.1 dBm. The IIP3 of a through line was also measured and is 68.3 dBm. The IIP3 is limited by the passive inter-modulation caused by the interface between the probe tips and CPW line and the substrate. The linearity limitation is typically found in probing RF MEMS switches [22].

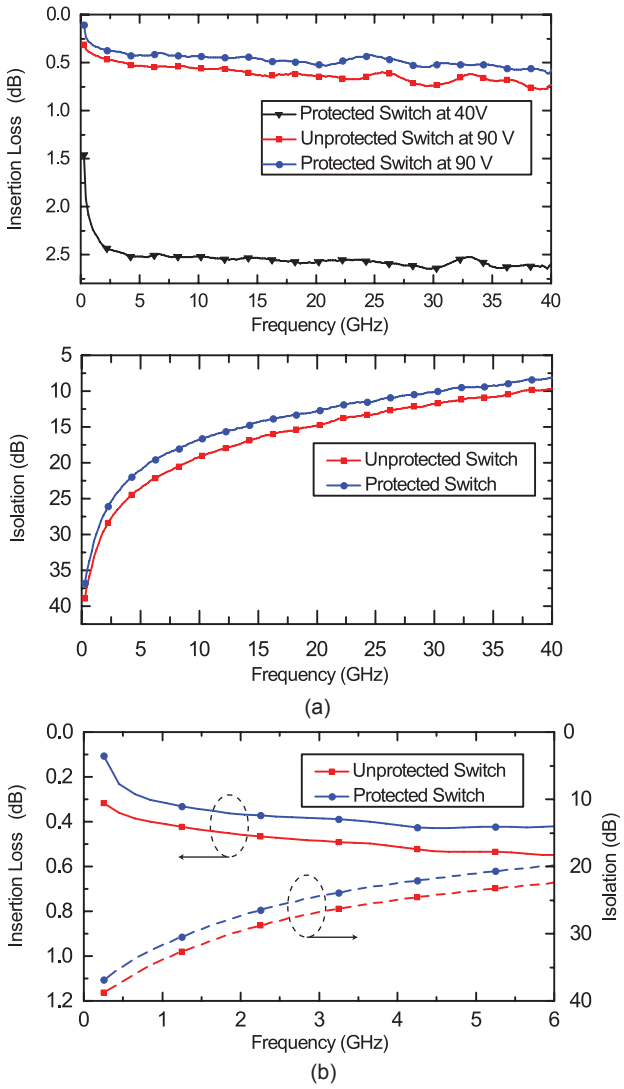

Fig. 16. (a) Measured S-parameters, (b) Zoom in of (a) from 0 GHz - 6 GHz

D. Switching time

The switching time was measured in order to set up the cycling frequency of the lifetime measurements. The test setup [Fig. 18(a)] consists of an RF signal generator, a circulator to block the reflected power, a function generator to generate the actuation waveform, a linear amplifier to amplify the waveform, an RF detector to convert the RF signal to dc signal, and an oscilloscope to capture the detected waveforms. When the switch is opened, the RF power is reflected and circulated to the $50\,\Omega$ load. Once the switch is closed, the RF power passes through the switch and is converted to dc voltage by the RF detector. The actuation waveform and detected waveform are compared in the oscilloscope to determine the switching time. The RF signal was set to 5 dBm at 2.4 GHz. A square waveform of 500 Hz, 5V peak to peak voltage, with a 20% duty cycle is supplied by the function generator. The waveform was amplified by 20 times in a linear amplifier.

A protected switch and an unprotected switch were measured in open air lab environment at room temperature. The

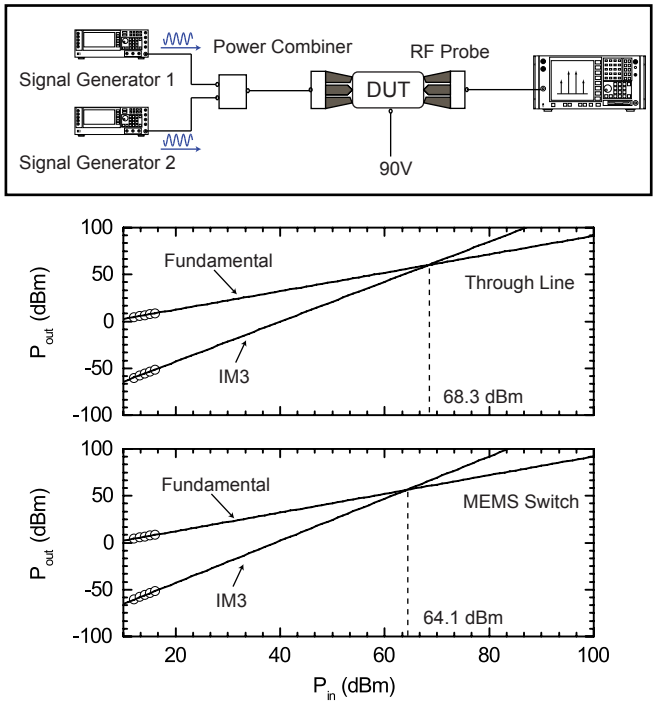

Fig. 17. Linearity test setup schematics and measured IIP3 for both through line and MEMS switch.

protected switch has a switch-on time of 45.1 µs and a switch-off time of 17.4 µs [Fig. 19 (a&b)]. The unprotected switch has on and off switching time of 49.7 µs and 9.6 µs [Fig. 19 (c&d)]. From the waveform, it can be seen that the switch has no bouncing when switching on or off.

E. Mechanical cycle test

To further isolate the failure mechanisms that are unique to electrical and mechanical phenomena, a switch with no RF power passing through was toggled to 500 million cycles to examine the mechanical impact damage of the dimple to the bottom electrode. A 4-point resistance measurement setup was used to measure the change of the contact resistance for both contacts. Fig. 20 shows the contact resistance changes over 500 million cycles. The contact resistance remained low up to 200 million cycles (9.52 Ω for protection contact and 1.87 Ω for low-resistance contact) and greatly increased after 500 million cycles (26.8 Ω for protection contact and 16.4 Ω for low-resistance contact). The increase of the contact resistance is due to the impact damage of the dimple to the bottom electrode.

F. Hot-switching lifetime

The hot-switching lifetime test setup is shown in Fig. 18(b). In addition to the switching time test setup, a power amplifier is included to amplify the input RF signal, a power meter is added to monitor the exact power level sent into the switch and a 4-point resistance measurement setup is connected through bias-Tee to consistently monitor changes in the contact resistance. The RF frequency used in the cycling test is

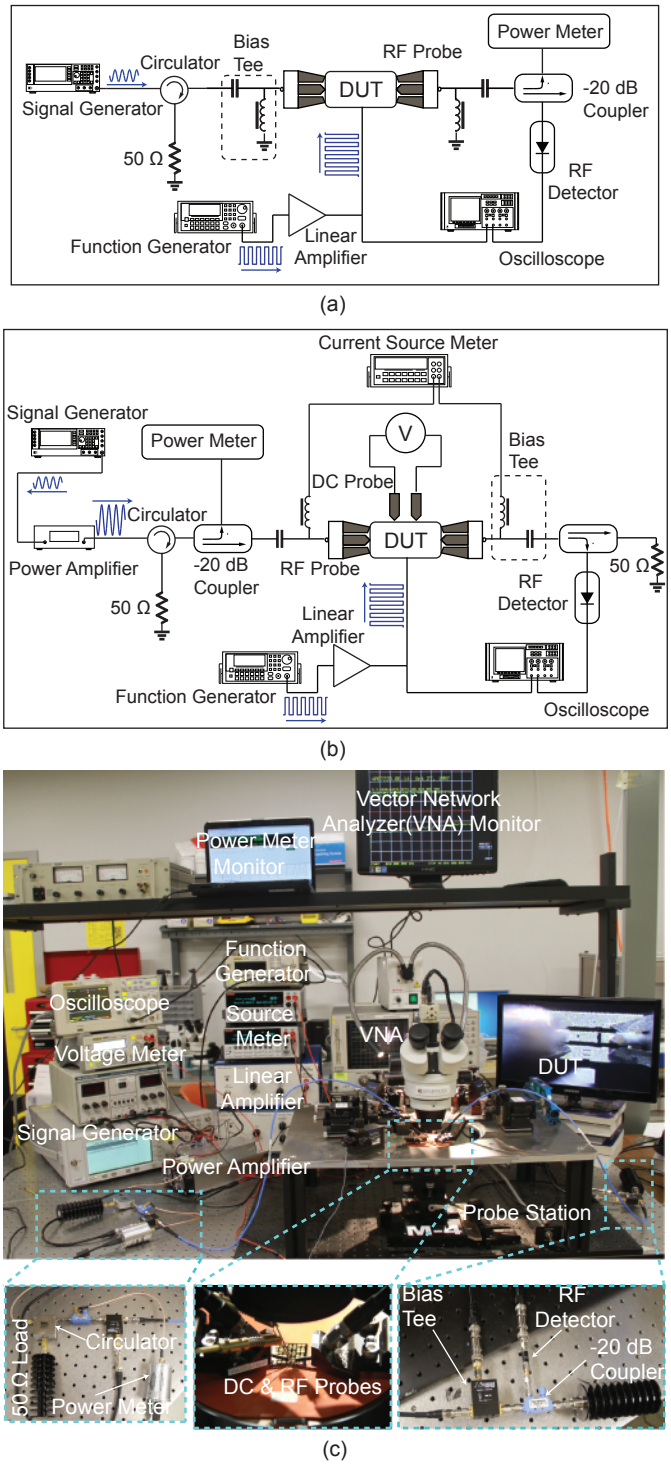

Fig. 18. (a) Test setup schematics for switching time measurement, (b) test setup schematics for hot-switching lifetime characterization, (c) test bench photo for S-parameters, switching time and reliability measurement.

2.4 GHz. The RF probes are used as the current source and two additional dc probes are used to measure the voltage drop across the switch. The contact resistance is measured by actuating the switch at 90 V using a dc voltage source (not shown in the figure). The dc probes do not touch the switch during cycling test and only touch the switch when

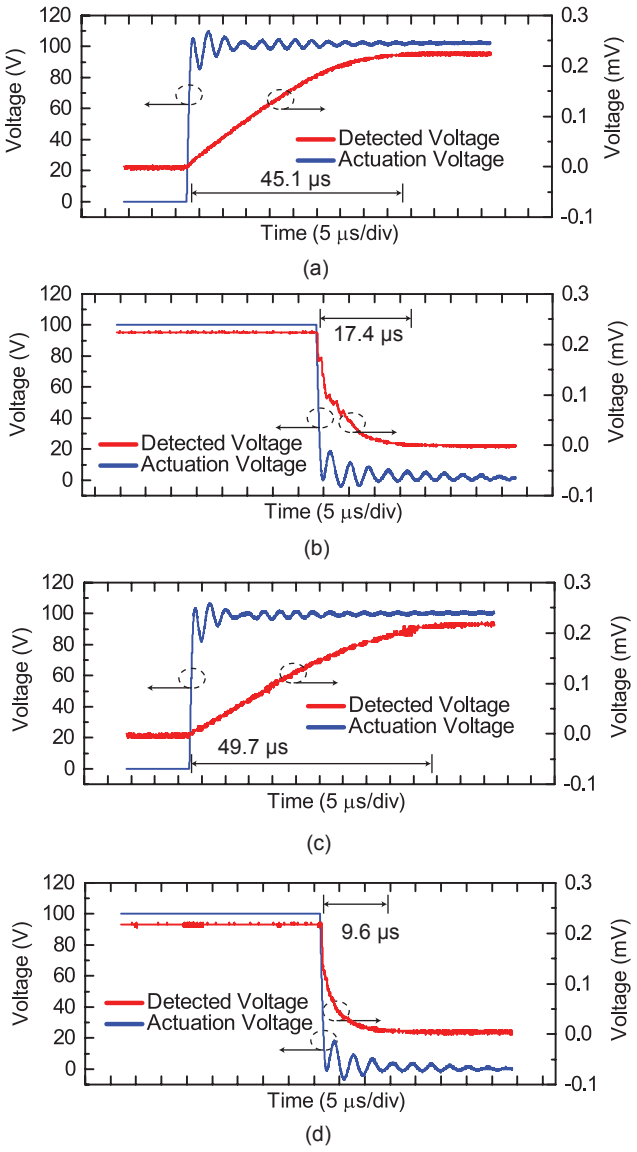

Fig. 19. (a) Switching-on time of protected switch, (b) switching-off time of protected switch, (c) switching-on time of unprotected switch, (d) switching-off time of unprotected switch.

resistance measurement is taken in order to isolate the potential RF signal leak from dc probes. The oscilloscope and the RF detector are used to detect the switching behavior changes. A total of six pairs of protected and unprotected switches are tested. Three pairs are tested under 1 W RF power and the other three 2 W, all under the hot-switching condition. Again, switches are tested under open air lab environment and room temperature conditions. The protected switches can all cycle up to 100 million cycles at 1 W and 50 million cycles under 2 W. Four pairs of protected and unprotected switches were measured continuously at 3 kHz and 50% duty cycle, while the other two pairs were measured at 1 kHz and 50% duty cycle and stopped at different cycle numbers to record the changes in contact resistance. All the contact resistance values were measured by the 4-point resistance measurement setup and the current source-meter was set to 5 mA for all resistance

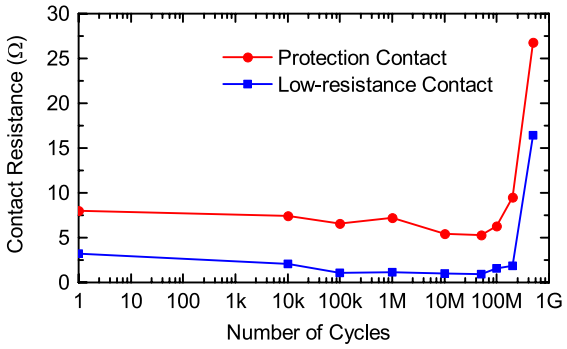

Fig. 20. Contact resistance changes of the protection contact and low-resistance contact over 500 million mechanical cycles.

measurements. It takes 9 hours and 27 hours to cycle a switch to 100 million cycles at 3 kHz and 1 kHz respectively. Due to time constraint, only two pairs (total four switches) were measured with contact resistance changes recorded.

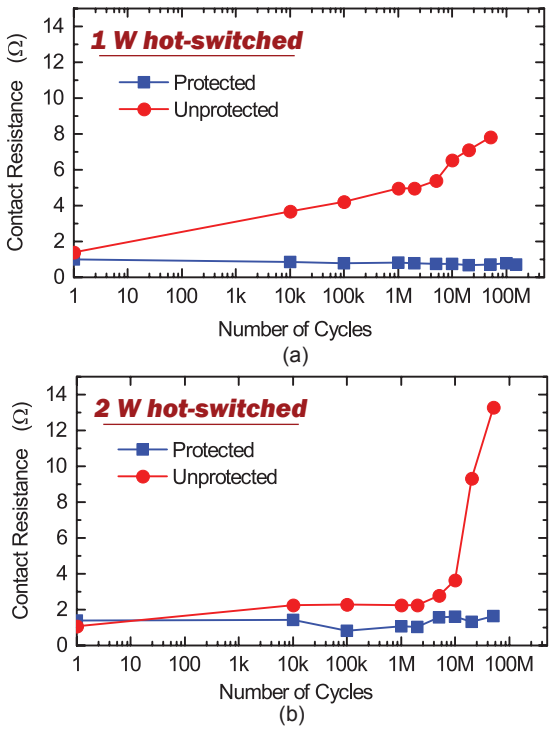

Fig. 21. (a) Measured contact resistances of switches pair under 1 W of different cycling numbers, (b) contanct resistances of switches pair under 2 W of different cycling numbers.

Fig. 21 (a) shows the contact resistance changes under 1 W hot-switching. The resistance of the low-resistance contacts was protected and remained below 1 Ω up to 100 million cycles, whereas that of the unprotected one increased beyond 1 Ω after approximately 10,000 cycles. Fig. 21(b) shows the contact resistance change under 2 W hot-switching. The same measurement setup was used. The low-resistance contacts on the protected switch remained below 1 Ω up to 50 million cycles, whereas the resistance of the unprotected one increased

TABLE II
COMPARISON OF SWITCH LIFETIME UNDER HOT-SWITCHING CONDITION

Design	Frequency Range (GHz)	Switching Power (W)	Cycling number
[22]	0–40	0.1	100 000 000
[23]	0–40	1	100 000 000
[25]	DC	0.1	100 000
[26]	DC	0.25	100 000
[4]	0–40	0.1	1000
This work	0–40	1	100 000 000
This work	0–40	2	50 000 000

beyond 1 Ω after approximately 10,000 cycles.

Both of the protected switches failed due to stiction at the protection contacts. The stiction failure was observed between 100 million to 150 million cycles under 1 W and 50 million to 100 million under 2 W. The stiction may be attributed to the local heating and melting of the contact material as the protection contact resistance increased. To alleviate the stiction problem, high contact force and restoring force actuator design can be used [22]. From the calculation in the mechanical design section, the cantilever tip will bend up if the biasing voltage keeps increasing. The bending of the tip can pull the protection dimple away from the bottom electrode. The switch can be actuated under higher biasing voltage to have the protection contact lifted up, in this case the protection contact will not participate in conducting current, leading to less local heating and melting problem and may also alleviate the stiction problem. Table II compares the lifetime of the proposed switch against recent demonstrations of hot-switching RF-MEMS switches. The switch shows state of the art reliability under hot-switching power of 1 W and great promise for the reliability under hot-switching power beyond 1 W.

VI. CONCLUSION

An RF-MEMS switch with series protection contact achieving high reliability under high power, hot-switching condition has been demonstrated. The series protection technique can boost hot-switching lifetime up to 100 times, compared with switches without series protection contacts. To further improve the reliability of the proposed switches, future work includes optimization of the structural design and contact materials.

ACKNOWLEDGMENT

The authors would like to thank staff members in Center for Nano-Micro Manufacturing (CNM2) at the Unversity of California, Davis, for help on device fabrication, and Mr. Hao Wang for help on device characterization.

REFERENCES

[1] G. M. Rebeiz and J. B. Muldavin, "RF MEMS switches and switch circuits," *Microwave Magazine, IEEE*, vol. 2, no. 4, pp. 59–71, 2001.

[2] M. Sakata, Y. Komura, T. Seki, K. Kobayashi, K. Sano, and S. Horiike, "Micromachined relay which utilizes single crystal silicon electrostatic actuator," in *Twelfth IEEE International Conference on Micro Electro Mechanical Systems*, 1999, Conference Proceedings, pp. 21–24.

[3] P. M. Zavracky, N. E. McGruer, R. H. Morrison, and D. Potter, "Microswitches and microrelays with a view toward microwave applications," *International Journal of RF and Microwave Computer-Aided Engineering*, vol. 9, no. 4, pp. 338–347, 1999.

[4] *Radant MEMS product brochure*, Radant MEMS, 2013. [Online]. Available: http://www.radantmems.com/radantmems/products.html

[5] *DelfMEMS product brochure*, DelfMEMS, 2015. [Online]. Available: http://www.delfmems.com/technology-rf-mems

[6] D. Peroulis, S. Pacheco, and L. Katehi, "RF MEMS switches with enhanced power-handling capabilities," *Microwave Theory and Techniques, IEEE Transactions on*, vol. 52, no. 1, pp. 59–68, Jan 2004.

[7] H. Zareie and G. Rebeiz, "Compact High-Power SPST and SP4T RF MEMS Metal-Contact Switches," *IEEE Transactions on Microwave Theory and Techniques*, vol. 62, no. 2, pp. 297–305, Feb 2014.

[8] S. Gong, H. Shen, and N. Barker, "Study of Broadband Cryogenic DC-Contact RF MEMS Switches," *IEEE Transactions on Microwave Theory and Techniques*, vol. 57, no. 12, pp. 3442–3449, Dec 2009.

[9] G. M. Rebeiz, C. D. Patel, S. K. Han, K. Chih-Hsiang, and K. M. J. Ho, "The Search for a Reliable MEMS Switch," *IEEE Microwave Magazine*, vol. 14, no. 1, pp. 57–67, 2013.

[10] M. Vincent, S. W. Rowe, C. Poulain, D. Mariolle, L. Chiesi, F. Houz, and J. Delamare, "Field emission and material transfer in microswitches electrical contacts," *Applied Physics Letters*, vol. 97, no. 26, pp. –, 2010.

[11] H. Kwon, D.-J. Choi, J.-H. Park, H.-C. Lee, Y.-H. Park, Y.-D. Kim, H.-J. Nam, Y.-C. Joo, and J.-U. Bu, "Contact materials and reliability for high power RF-MEMS switches," *MEMS. IEEE 20th International Conference on Micro Electro Mechanical Systems*, pp. 231–234, Jan 2007.

[12] M. H. David Becher, Richard Chan and M. Feng, "Reliability Study of Low-Voltage RF MEMS Switches," *GaAs MANTECH*, pp. 54–7, 2002.

[13] S. Patton and J. Zabinski, "Fundamental studies of Au contacts in MEMS RF switches," *Tribology Letters*, vol. 18, no. 2, pp. 215–230, 2005.

[14] Z. Yang, D. Lichtenwalner, A. Morris, J. Krim, and A. I. Kingon, "Contact degradation in hot/cold operation of direct contact microswitches," *Journal of Micromechanics and Microengineering*, vol. 20, no. 10, p. 105028, 2010.

[15] D. A. Czaplewski, C. D. Nordquist, C. W. Dyck, G. A. Patrizi, G. M. Kraus, and W. D. Cowan, "Lifetime limitations of ohmic, contacting RF MEMS switches with Au, Pt and Ir contact materials due to accumulation of friction polymer on the contacts," *Journal of Micromechanics and Microengineering*, vol. 22, no. 10, p. 105005, 2012.

[16] J. Maciel, S. Majumder, J. Lampen, and C. Guthy, "Rugged and reliable ohmic MEMS switches," *2012 IEEE MTT-S International Microwave Symposium Digest (MTT)*, pp. 1–3, June 2012.

[17] D. A. Czaplewski, C. D. Nordquist, G. A. Patrizi, G. M. Kraus, and W. D. Cowan, "RF MEMS Switches With RuO2/Au Contacts Cycled to 10 Billion Cycles," *Journal of Microelectromechanical Systems*, vol. 22, no. 3, pp. 655–661, 2013.

[18] J. Costa. RF MEMS switch technology for radio front end applications. RFMD. [Online]. Available: http://www.rfmd.com/sites/default/files/resources/migration/presentations/CommJCostaRWS10Presentation.pdf

[19] R. P. Hennessy, A. Basu, G. G. Adams, and N. E. McGruer, "Hot-switched lifetime and damage characteristics of MEMS switch contacts," *Journal of Micromechanics and Microengineering*, vol. 23, no. 5, p. 055003, 2013.

[20] T. Ishida, K. Kakushima, and H. Fujita, "Degradation Mechanisms of Contact Point During Switching Operation of MEMS Switch," *Journal of Microelectromechanical Systems*, vol. 22, no. 4, pp. 828–834, 2013.

[21] A. Basu, R. Hennessy, G. Adams, and N. McGruer, "Reliability in Hot Switched Ruthenium on Ruthenium MEMS Contacts," in *2013 IEEE 59th Holm Conference on Electrical Contacts (HOLM)*, 2013, Conference Proceedings, pp. 1–8.

[22] C. D. Patel and G. M. Rebeiz, "A High-Reliability High-Linearity High-Power RF MEMS Metal-Contact Switch for DC to 40-GHz Applications," *IEEE Transactions on Microwave Theory and Techniques*, vol. 60, no. 10, pp. 3096–3112, 2012.

[23] L. L. W. Chow, J. L. Volakis, K. Saitou, and K. Kurabayashi, "Lifetime Extension of RF MEMS Direct Contact Switches in Hot Switching Operations by Ball Grid Array Dimple Design," *IEEE Electron Device Letters*, vol. 28, no. 6, pp. 479–481, 2007.

[24] L. Yuhao, Y. Bey, and L. Xiaoguang, "Single-actuator shunt-series RF-MEMS switch," in *2014 IEEE MTT-S International Microwave Symposium (IMS)*, 2014, Conference Proceedings, pp. 1–4.

[25] S. Yong-Ha, K. Min-Wu, L. Jeong Oen, K. Seung-Deok, and Y. Jun-Bo, "Complementary Dual-Contact Switch Using Soft and Hard Contact Materials for Achieving Low Contact Resistance and High Reliability

Simultaneously," *Journal of Microelectromechanical Systems*, vol. 22, no. 4, pp. 846–854, 2013.
[26] S. Yong-Ha, K. Min-Wu, S. Min-Ho, and Y. Jun-Bo, "A complementary dual-contact mems switch using a zipping technique," *Journal of Microelectromechanical Systems*, vol. 23, no. 3, pp. 710–718, 2014.
[27] J. M. Gere and S. P. Timoshenko., *Mechanics of Materials*, 4th ed., 1997.
[28] G. M. Rebeiz, *RF MEMS: Theory, Design, and Technology*. Wiley, 2003.
[29] H.-H. Hsu, M. Koslowski, and D. Peroulis, "An Experimental and Theoretical Investigation of Creep in Ultrafine Crystalline Nickel RF-MEMS Devices," *IEEE Transactions on Microwave Theory and Techniques*, vol. 59, no. 10, pp. 2655–2664, Oct 2011.
[30] *Coventorware10*, Coventor Inc., 2015. [Online]. Available: www.coventor.com
[31] *ANSYS HFSS*, ANSYS, Inc., 2015. [Online]. Available: http://www.ansys.com/Products/Simulation+Technology/Electronics/Signal+Integrity/ANSYS+HFSS